











Multiple Genomic Landscapes of Recombination and Genomic Divergence in Wild Populations of House Mice—The Role of Chromosomal Fusions and *Prdm9*

Cristina Marín-García ^{1,2}, Lucía Álvarez-González ^{1,2}, Laia Marín-Gual ^{1,2}, Sònia Casillas ^{2,3}, Judith Picón ^{1,2}, Keren Yam ^{1,2}, María Magdalena Garcias-Ramis ^{1,2}, Covadonga Vara ^{1,2}, Jacint Ventura ^{4,5} and Aurora Ruiz-Herrera ^{1,2,*}

¹Departament de Biologia Cel·lular, Fisiologia i Immunologia, Universitat Autònoma de Barcelona, Cerdanyola del Vallès 08193, Barcelona, Spain

²Institut de Biotecnologia i Biomedicina, Universitat Autònoma de Barcelona, Cerdanyola del Vallès 08193, Barcelona, Spain

³Departament de Genètica i Microbiologia, Universitat Autònoma de Barcelona, Cerdanyola del Vallès 08193, Barcelona, Spain

⁴Departament de Biologia Animal, Biologia Vegetal i Ecologia, Universitat Autònoma de Barcelona, Cerdanyola del Vallès 08193, Barcelona, Spain

⁵Small Mammals Research Unit, Granollers Museum of Natural Sciences, Granollers 08402, Barcelona, Spain

*Corresponding author: E-mail: aurora.ruizherrera@uab.cat.

Associate editor: Amanda Larracuent

Abstract

Chromosomal fusions represent one of the most common types of chromosomal rearrangements found in nature. Yet, their role in shaping the genomic landscape of recombination and hence genome evolution remains largely unexplored. Here, we take advantage of wild mice populations with chromosomal fusions to evaluate the effect of this type of structural variant on genomic landscapes of recombination and divergence. To this aim, we combined cytological analysis of meiotic crossovers in primary spermatocytes with inferred analysis of recombination rates based on linkage disequilibrium using single nucleotide polymorphisms. Our results suggest the presence of a combined effect of Robertsonian fusions and *Prdm9* allelic background, a gene involved in the formation of meiotic double strand breaks and postzygotic reproductive isolation, in reshaping genomic landscapes of recombination. We detected a chromosomal redistribution of meiotic recombination toward telomeric regions in metacentric chromosomes in mice with Robertsonian fusions when compared to nonfused mice. This repatterning was accompanied by increased levels of crossover interference and reduced levels of estimated recombination rates between populations, together with high levels of genomic divergence. Interestingly, we detected that *Prdm9* allelic background was a major determinant of recombination rates at the population level, whereas Robertsonian fusions showed limited effects, restricted to centromeric regions of fused chromosomes. Altogether, our results provide new insights into the effect of Robertsonian fusions and *Prdm9* background on meiotic recombination.

Key words: Robertsonian fusions, recombination, crossovers, *Prdm9*, genomic divergence, *Mus musculus domesticus*.

Introduction

Determining the genomic basis of speciation is a research priority in biology. In this context, understanding the origin and evolutionary plasticity of gross structural genome reorganizations, such as inversions and fusions, is key. Models and growing experimental evidence suggest that chromosomal rearrangements are relevant in adaptation and speciation (Kirkpatrick 2010; Mackintosh et al. 2023; Mérot et al. 2023; Yoshida et al. 2023). This is now facilitated by the availability of unprecedented genomic resources that allow studying the effect of genome

reorganizations on selection, gene flow, drift, mutation rate, and recombination. Previous studies of inversions have evidenced genomic divergence and reduced recombination in plants, fish, birds, and insects (reviewed in Wellenreuther and Bernatchez 2018). However, the impact of balanced inter-chromosomal rearrangements, such as chromosomal fusions, on genome architecture and its heritability is less explored, especially in natural populations.

Chromosomal fusions represent one of the most common types of chromosomal rearrangements in nature, widely present in plants and animals (White 1973; King 1995); yet

Received: November 06, 2023. **Revised:** February 21, 2024. **Accepted:** March 14, 2024

© The Author(s) 2024. Published by Oxford University Press on behalf of Society for Molecular Biology and Evolution.

This is an Open Access article distributed under the terms of the Creative Commons Attribution-NonCommercial License (<https://creativecommons.org/licenses/by-nc/4.0/>), which permits non-commercial re-use, distribution, and reproduction in any medium, provided the original work is properly cited. For commercial re-use, please contact reprints@oup.com for reprints and translation rights for reprints. All other permissions can be obtained through our RightsLink service via the Permissions link on the article page on our site—for further information please contact journals.permissions@oup.com.

Open Access

their impact on recombination and genome divergence is underexplored. This is especially relevant for Robertsonian (Rb) fusions, which result when two telocentric or acrocentric chromosomes fuse through the centromere resulting in one metacentric chromosome (Robertson 1916). Theoretical work has predicted that chromosomal fusions can facilitate adaptation by bringing together previously unlinked loci (Guerrero and Kirkpatrick 2014). This complements initial experimental work reporting an overall reduction and chromosomal redistribution of recombination in fused chromosomes, either by cytological approaches (Bidau et al. 2001; Castiglia and Capanna 2002; Dumas and Britton-Davidian 2002; Capilla et al. 2014) or by estimations of gene flow (Franchini et al. 2010; Förster et al. 2013). More recent work has revealed that Rb fusions reshape recombination landscapes genome-wide (not only affecting fused chromosomes but also non-fused chromosomes) by remodeling the three-dimensional (3D) genome-wide topology in germ cells (Vara et al. 2021; Vara and Ruiz-Herrera 2022; Álvarez-González et al. 2022a). In this context, it has been suggested that lineage-specific chromosomal rearrangements can impose structural constraints (i.e. acting as barriers for genomic contacts with surrounding regions inside the nucleus), thus acting as “structural genomic islands” of divergence (Álvarez-González et al. 2022b). This line of evidence suggests that structural genomic rearrangements can impose topological barriers from the surrounding chromosomal regions, with potential functional implications for evolution, including recombination.

Meiotic recombination is a tightly regulated process that generates genetic variability and ensures segregation of homologous chromosomes. Several regulatory mechanisms are involved in the generation of controlled double strand breaks (DSBs) by SPO11 during early stages of meiosis (Keeney et al. 1997; Romanienko and Camerini-Otero 2000). Among other factors, the *Prdm9* gene encodes for a meiotic-specific histone methyltransferase that trimethylates H3 (H3K4me3 and H3K36me3), predetermining the localization of SPO11-driven DSBs (Mihola et al. 2009; Baudat et al. 2010; Parvanov et al. 2010; Smagulova et al. 2011; Diagouraga et al. 2018). This is achieved by the recognition of species-specific DNA motifs by the C-terminal tandem repeat Zinc Finger (ZnF) array (Berg et al. 2010). PRDM9 binding sites occupy intervals across the genome facilitating the placement of DSBs (Smagulova et al. 2011; Paigen and Petkov 2018; Tock and Henderson 2018), of which the majority (90%) are repaired as noncrossovers and the remaining (10%) as crossovers (COs) in mice (Li et al. 2019; Gergelits et al. 2021). *Prdm9* is characterized by being highly polymorphic due to the variability of the ZnF array, presenting inter-individual differences in both the number of ZnF conforming the array and sequence of three positions of each repeat that are the most variable (position -1, +3, and +6), the so-called “hypervariable” sites (Baudat et al. 2010). In the case of the genus *Mus* (i.e. *Mus musculus domesticus* and *Mus minutoides*), more than 150 alleles

have been described in wild populations (Buard et al. 2014; Capilla et al. 2014; Kono et al. 2014; Vara et al. 2019).

ZnF polymorphisms result in an allele-specific hotspot distribution, a pattern found in different mammalian species, including humans, nonhuman primates, cattle, and mice (Berg et al. 2010, 2011; Brick et al. 2012; Groeneveld et al. 2012; Sandor et al. 2012). During early stages of meiosis, the PRDM9 protein forms a heterodimeric complex necessary to recognize specific DNA motifs (Schwarz et al. 2019) that can result in competition between different alleles, affecting both the number and chromosomal distribution of DSBs (Baker et al. 2015). Notably, *Prdm9* allelic variability can be involved in reproductive postzygotic isolation since asymmetric DSBs (meaning different numbers and distribution of DSBs between homologous chromosomes) can account for synapsis failure during meiosis resulting in subfertile and even sterile phenotypes (Gregorova et al. 2018). In fact, *Prdm9* has been considered a speciation gene for mammals as it can be involved in hybrid sterility in mice (Mihola et al. 2009). In addition to the high percentage of *Prdm9* heterozygotic mice described in natural populations (Buard et al. 2014; Kono et al. 2014; Vara et al. 2019), the hypervariable positions of ZnF present significant deviation from Hardy–Weinberg equilibrium, suggesting the effect of positive selection (due to evolutionary dynamics such as bottlenecks and/or functional constraints) (Vara et al. 2019). It is not completely understood, however, the effect of the natural variability of *Prdm9* on meiotic recombination and its possible mechanistic and genetic constraints.

Rb fusions are present in wild populations of *M. m. domesticus* and represent a distinctive model to study the effect of *Prdm9* allelic background and chromosomal rearrangements and their impact on fertility and evolution (Piálek et al. 2005; Medarde et al. 2012; Capilla et al. 2014; Vara et al. 2021). Along the geographic distribution of this taxon, there are many areas in which populations with different sets of metacentric chromosomes hybridize with each other and/or with standard (*St*) populations ($2n = 40$), which jointly comprise the so-called Rb systems (Piálek et al. 2005). Among them, the Barcelona Robertsonian System (BRbS) is located, in an area of approximately 5,000 km², in the Northeastern area of the Iberian Peninsula (Gündüz et al. 2001; Medarde et al. 2012). This Rb area is a unique model from all other Rb systems of the house mouse, since there is not an exclusive Rb race and the set of metacentrics detected to date [(Rb(3.8), Rb(4.14), Rb(5.15), Rb(6.10), Rb(7.17), Rb(9.11), and Rb(12.13)] are geographically distributed following a staggered clinal pattern (Gündüz et al. 2001; Medarde et al. 2012). The resulting geographic clines leads to a progressive reduction in diploid numbers toward the center of the range giving place to diploid numbers ranging from $2n = 39$ to $2n = 27$, surrounded by *St* populations (Medarde et al. 2012).

Although initial reports detected a reduction of recombination rates (RR) in Rb populations when compared with *St* populations in the BRbS (Capilla et al. 2014;

Vara et al. 2021), the mechanism behind this pattern is not fully understood. In the present work, we combine the cytological analysis of COs by immunofluorescence with the analysis of inferred RRs based on linkage disequilibrium (LD) using single nucleotide polymorphism (SNPs) data to disentangle the effect of structural (Rb fusions) and genetic factors (*Prdm9* allelic background) in the remodeling recombination landscapes in wild populations.

Results

Rb Fusions Increase Genetic Differentiation in Wild Populations

Genetic structure analysis revealed a clear clustering of St populations (Castellfollit del Boix, CFBSt; Castellar del Vallès, CTRSt) with a distinctive genetic differentiation between Rb populations (Sant Sadurní d'Anoia, SS^{Rb}; Castelldefels, CS^{Rb}; Viladecans, VDC^{Rb}) (Fig. 1, a and b; supplementary table S1, Supplementary Material online). This population structure was confirmed by admixture analysis (Fig. 1c). For ancestry $K = 4$, Rb populations presented differentiated ancestry when compared to St populations. When analyzing ancestry $K = 5$, each population showed a specific ancestry, corresponding to their geographical distribution. Importantly, the phylogenetic analysis following the neighbor-joining approach (Fig. 1d) revealed that St populations (CFBSt and CTRSt) are present at a branch of the tree sharing a common ancestor, from which the Rb population with the lowest number of fusions (SS^{Rb}) diverge. Rb populations with a high number of fusions (CS^{Rb} and VDC^{Rb}) shared a common clade but with a distant ancestor. Although the analysis of general parameters of genomic diversity (supplementary table S2, Supplementary Material online) did not show substantial differences between populations, genome-wide analysis of genomic differentiation (expressed as weighted F_{ST} values) revealed high rates of differentiation for VDC^{Rb} (the population with the highest number of Rb fusions) when compared to most populations (Fig. 1, e and f). Genetic differentiation (F_{ST}), however, was not correlated with geographical distance (expressed as kilometres) ($R^2 = 0.0008$, P -value = 0.98), suggesting a role of Rb fusions in generating divergence.

High Variability of *Prdm9* in Wild Mice

Since *Prdm9* polymorphisms can influence genomic landscapes of recombination (Paigen and Petkov 2018), we analyzed *Prdm9* allelic variability in wild mice (Fig. 2a; supplementary table S3, Supplementary Material online). Previous studies have showed a high *Prdm9* variation in natural populations of house mice, identifying nearly 60 different alleles (Kono et al. 2014; Vara et al. 2019). The present survey resulted in the identification of five new alleles (9A, 10L, 12P, 13K, and 13L) (Fig. 2a) in addition to four alleles (10A, 12I, 13A, and 11S) previously described in the BRBs (Capilla et al. 2014; Vara et al. 2019). The St population CFBSt showed the highest allelic variability (Fig. 2b),

with 48% of mice heterozygous for different alleles. The most frequently detected allele in CFBSt was 10A (40%) mirroring previous studies (Vara et al. 2019), either in homozygosity or in combination with minor alleles. Remarkably, there was a high prevalence of the 10A allele in homozygous state in Rb populations (between 80% and 100%). Remarkably, both St populations (CTRSt and CFBSt) showed distinctive features in terms of *Prdm9* background (Fig. 2b). Whereas mice from CFBSt had different *Prdm9* allelic combinations, mice from CTRSt presented mainly the 10A allele, either in the homozygous state or combined with the 13K allele.

We further analyzed whether selection played a role in shaping *Prdm9* allelic variability on each population by applying different selection tests (supplementary table S4, Supplementary Material online). Fu-Li's D showed that CFBSt presents an excess of ancestral variants that might have been subjected to past selection events (P -value < 0.02). Tajima's D showed that both CTRSt and VDC^{Rb} present high number of rare alleles (P -value < 0.02 and P -value < 0.05, respectively), which is indicative of recent selection. The McDonald–Kreitman selection test showed an excess of nonsynonymous polymorphism in CFBSt (P -value < 0.05), with a Neutrality Index (NI) larger than 1. Consequently, the analysis of nucleotide diversity (π) in synonymous (π_s) and nonsynonymous (π_a) sites also showed that most of the nucleotide diversity resides in aminoacidic-replacement sites, with π_a/π_s values much larger than 1.

Since the initial repeats of the ZnF array (from ZnF3 to ZnF6) are known to contribute to the binding of PRDM9 to the DNA, hence determining the location of meiotic DSBs (Billings et al. 2013; Baker et al. 2015; Paigen and Petkov 2018), we also calculated π per codon and observed that most of the nucleotide diversity resides in the hyper-variable positions -1 , $+3$, and $+6$ (P -value = 3.11×10^{-6} , P -value = 2.19×10^{-5} , and P -value = 0.00337 for the ZnF3 to ZnF6 region in the CFBSt, CTRSt, and VDC^{Rb} populations, respectively; Fig. 2c). Altogether, the St population CTRSt, despite not having chromosomes fused, shared similarities with Rb populations in terms of *Prdm9* allelic background, suggesting a common ancestry. This was also evidenced by the phylogenetic analysis (Fig. 1d).

Redistribution of COs across Chromosomal Axes

We further studied the effect of Rb fusions and *Prdm9* allelic diversity in remodeling recombination landscapes. To that aim, we first conducted a cytological analysis of the MLH1 protein (as a proxy of COs) on spermatocyte spreads (Fig. 3a). We detected significant differences in the number of COs per cell between populations (Wilcoxon test, P -value < 0.05, supplementary fig. S1A and supplementary table S5, Supplementary Material online). When considering the karyotype, St mice showed higher numbers of MLH1 foci per cell (mean values of 20.67 ± 1.4 COs per cell) than Rb mice (mean values of 19.97 ± 1.9 COs per cell) (t -test, P -value < 2×10^{-16} , supplementary fig. S1B, Supplementary Material online),

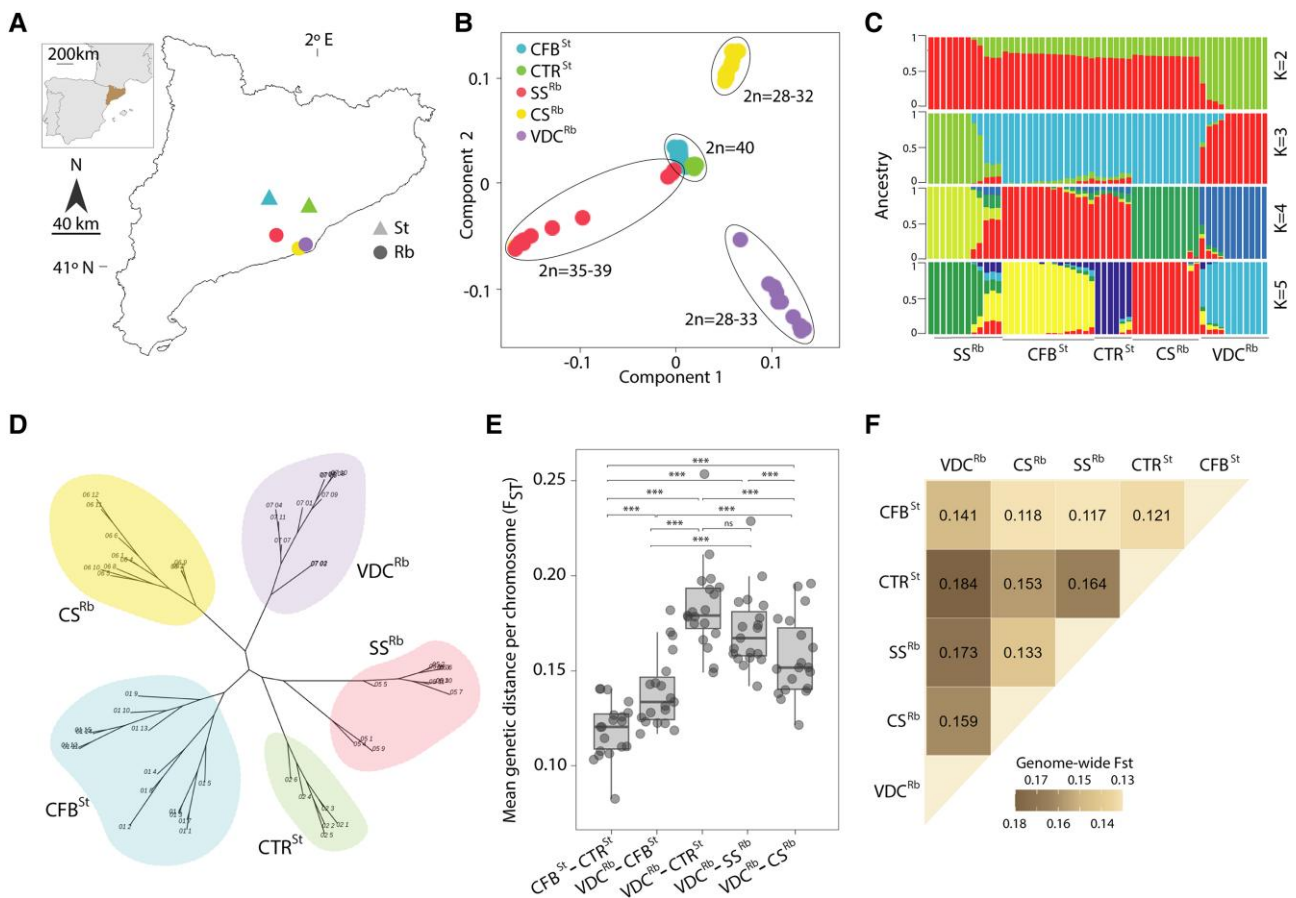


Fig. 1. Geographical distribution and population structure of wild mice populations. a) Geographical distribution of populations studied (see [supplementary table S1, Supplementary Material](#) online for details). b) PCA. Diploid numbers ($2n$) are indicated. c) Plots showing the proportion of inferred ancestry by ADMIXTURE for $K = 2$ to $K = 5$ in mice from panel b. d) Phylogenetic tree derived from panel b. e) Pairwise analysis of genetic distance (mean F_{ST}) between populations. Dots represent different mouse chromosomes. Wilcoxon pairwise test ($***P < 0.001$). f) Genome-wide pairwise analysis of genetic distance (mean F_{ST} values) between populations. Abbreviations: CFBSt, Castellfollit del Boix; CTRSt, Castellar del Vallès; CS^{Rb}, Castelledefells; SS^{Rb}, Sant Sadurn d'Anoia; VDC^{Rb}, Viladecans; St, standard mice; Rb, Robertsonian mice.

mirroring previous studies (Vara et al. 2021). Interestingly, the coefficient of variation (CV) of Rb populations was higher (9.4 ± 0.1) than in St populations (6.7 ± 0.2), indicating that Rb mice present more variation in the number of COs per cell than St mice ([supplementary table S5, Supplementary Material](#) online) probably due to a redistribution of COs due to the presence of Rb fusions.

When analyzing the effect of the *Prdm9* allele ([supplementary fig. S1C, Supplementary Material](#) online), we found that mice homozygous for the 10A allele present similar values of COs per cell, regardless of the presence of Rb fusions (Tukey's test, P -value > 0.07). Differences between populations were only found when the 10A *Prdm9* allele is present in heterozygosity or not present at all, suggesting a role of *Prdm9* background on recombination (Tukey's test, P -value $< 2 \times 10^{-16}$). In fact, a two-way ANOVA indicated the presence of a significant interaction between *Prdm9* allele background and COs per cell (F -value = 7.4, P -value = 6×10^{-5}).

We then analyzed more into detail the chromosomal distribution of COs in three populations (CFBSt, CTRSt, and VDC^{Rb}) to disentangle the relative contribution of

Rb fusions (Fig. 3). This allowed us to dissect the combinational effect of *Prdm9* allelic background and chromosomal rearrangements. On the one hand, CFBSt and CTRSt populations were homogeneous in their chromosome complement (no fusions) and genetic background (little genome differentiation as reflected by the PCA analysis) but presented different *Prdm9* allelic composition. On the other hand, CTRSt and VDC^{Rb} populations were homozygous for the 10A *Prdm9* allele but present different chromosome complement (St vs. Rb).

The analysis of the numbers of COs per arm (0, 1, or 2 COs) revealed differences between populations (Chi-square test, P -value < 0.001 , Fig. 3b). St populations CFBSt and CTRSt presented low proportions of arms with 0 COs (below 2% in both populations), ensuring the obligatory CO per arm to avoid chromosome missegregation (Jones and Franklin 2006). In Rb mice (VDC^{Rb} population), however, the proportion of arms with 0 COs showed a 3-fold increase (up to 6%) when compared with St mice. Moreover, when considering the proportion of arms with two COs, the St population with the highest proportion of chromosomal arms (11% in CFBSt) also presented

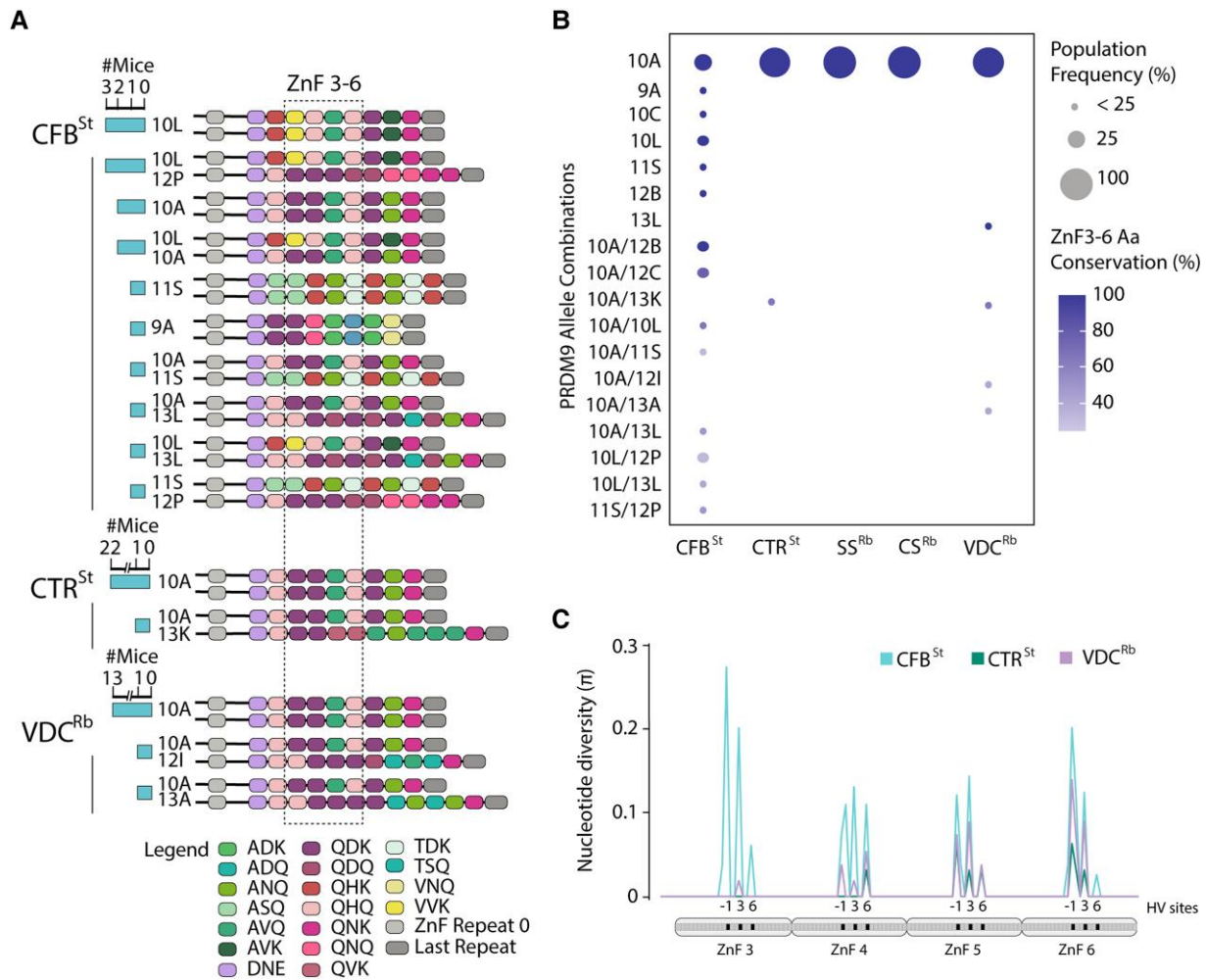


Fig. 2. *Prdm9* allele variability in wild mice from BRBS. a) Structure of the ZnF domains detected in this study. Legend indicates the amino acid (Aa) combination of the hypervariable positions (−1, +3, and +6) of each ZnF repeat. The discontinuous box includes ZnF3-6. b) Bubble plot displaying population allelic frequency and Aa conservation of hypervariable (HV) codons of ZnF3-6 per each population. c) Nucleotide diversity (π) per codon in ZnF3-6 (only populations showing nucleotide diversity are shown). Each rectangle represents each ZnF and each square represents a codon, with the HV codons −1, +3, and +6 marked in black. Abbreviations: CFBSt, Castellfollit del Boix; CTRSt, Castellar del Vallès; CS^{Rb}, Castelldefells; SS^{Rb}, Sant Sadurn d’Anoia; VDC^{Rb}, Viladecans; St, standard mice; Rb, Robertsonian mice.

the highest ratio of CO per cell ($20.9 \pm 1.4\%$) (Fig. 3b). Also, we detected a positive correlation between the number of COs and the length of the chromosomal arm in all three populations (Spearman correlation, P -value $< 2.2 \times 10^{-16}$, supplementary fig. S1D, Supplementary Material online). Altogether, these results indicate that high numbers of COs per cells was accompanied by a high proportion of chromosomal arms with two COs and longer chromosomal axes.

To fully understand the distribution of COs in Rb mice, we analyzed the proportions of COs considering three types of chromosomal arms: (i) acrocentric arms in Rb mice, (ii) metacentric chromosomes in the homozygous state, and (iii) metacentric chromosomes in the heterozygous state (supplementary fig. S1, E to I, Supplementary Material online). Our results showed that the arm type that mainly contributed to the zero proportion of COs were metacentric chromosomes in homozygous state

(10%), and to a lesser extent, metacentric chromosomes in heterozygous state (4%) (Chi-square test, P -value < 0.001 , supplementary fig. S1F, Supplementary Material online). Furthermore, the proportion of chromosomal arms with 2 foci were reduced in metacentric chromosomes (8%) when compared to acrocentric (11%). Interestingly, acrocentric chromosomes (nonfused chromosomes) in Rb mice were also affected when comparing to acrocentric chromosomes in St mice in terms of high percentage of arms with 0 foci (Chi-square test, P -value < 0.001 , Fig. 3b and supplementary fig. S1F, Supplementary Material online). Overall, these results suggest that recombination is affected genome-wide, involving all chromosomes including those not involved in Rb fusions.

We next analyzed the relative distance of COs from centromeres between populations and chromosomal arm types. When considering chromosomal arms with one MLH1 focus, COs tend to localize in interstitial and

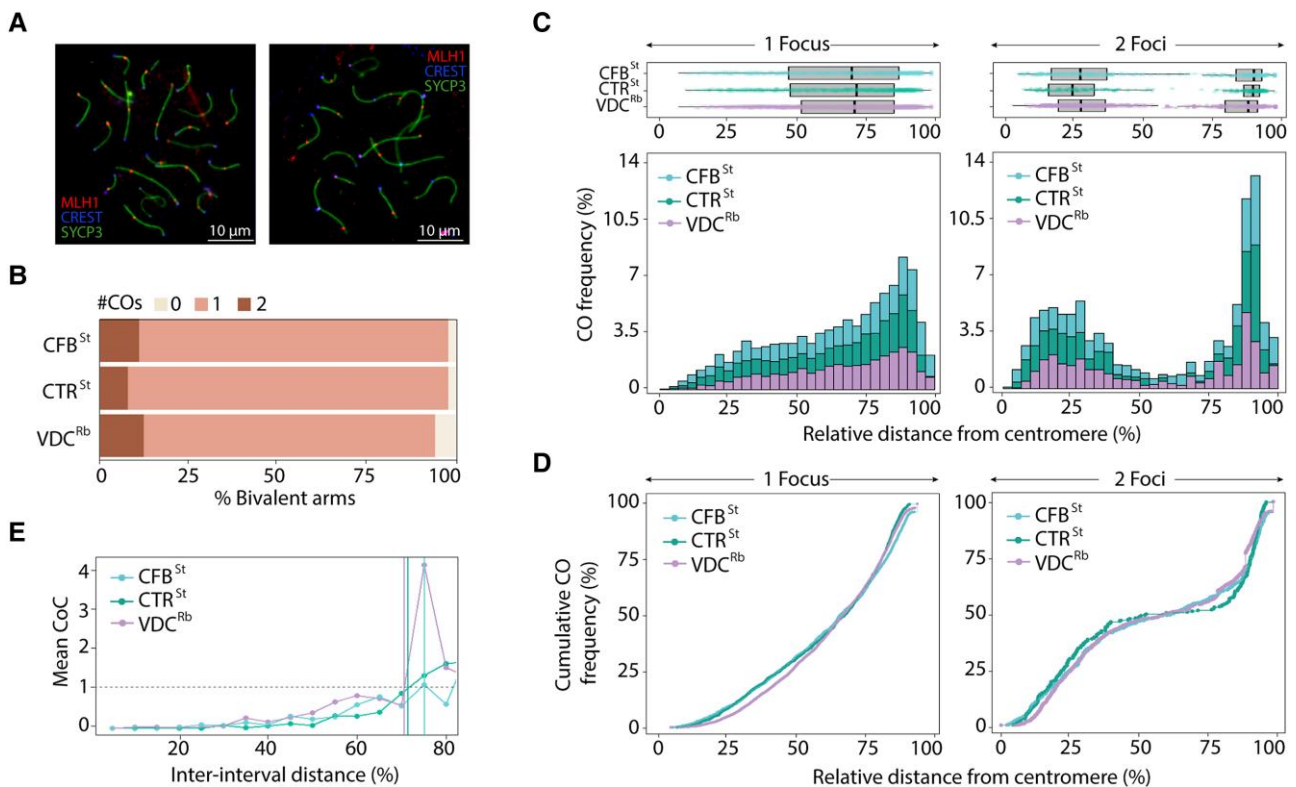


Fig. 3. Cytological analysis of recombination. a) Representative immunofluorescence images of primary spermatocytes at pachytene stage, labeling lateral elements of the synaptonemal complex (SYCP3), centromere (CREST), and meiotic crossovers (COs, MLH1) in standard (left) and Robertsonian (right) mice. b) Percentage of bivalent arms showing the numbers of COs per arm (Chi-square test, $P < 0.001$). Number of analyzed chromosomal arms: $CFB^{St} = 2,261$, $CTR^{St} = 1,862$, and $VDC^{Rb} = 5,472$. c) Distribution of COs across chromosomal axes relative to the centromere showing the median values of COs and deviation (upper panel) when considering 1 focus of MLH1 (left) or 2 foci (right). d) Cumulative frequency plots of COs from panels b and c. e) CoC curve. The horizontal line represents the expected level without interference (mean CoC = 1) whereas vertical lines represent the intercept. Abbreviations: CFB^{St} , Castellfollit del Boix; CTR^{St} , Castellar del Vallès; VDC^{Rb} , Viladecans.

telomeric regions (from 52% to 80% of the arm length) (Fig. 3c and supplementary fig. S1, E to G, Supplementary Material online). Differences between populations were evidenced by COs cumulative frequencies curves (Kolmogorov–Smirnov test, P -value < 0.005 , Fig. 3d) where Rb mice (VDC^{Rb}) showed reduced frequencies in proximal regions of the centromere when compared to both St populations (CTR^{St} and CFB^{St}), and thereby affecting the overall placement of COs in interstitial and distal regions. When considering chromosomal arms with two MLH1 foci, all three populations showed a bimodal distribution (Fig. 3c). That is, the first CO was detected proximal to the centromere (mean $29 \pm 13\%$ of the arm length), whereas the second CO was displaced toward terminal chromosomal regions (mean $88 \pm 9\%$ of the arm length).

Distinctive Patterns of CO Interference

We further investigated whether a relaxation of CO interference (COI) could account for the distinctive patterns of CO distribution observed. COI is the tendency of COs to form farther away from one another along the chromosome than would be expected by chance (reviewed in Girard et al. 2023). This analysis was conducted by fitting the relative positions of COs to a gamma distribution

and by analyzing of the coefficient of coincidence (CoC) (see Materials and Methods, supplementary table S6, Supplementary Material online). The gamma distribution is a useful model for estimating the presence and the strength of COI—this being reflected by the interference parameter (γ). The higher the γ value, the higher the influence of COI, being $\gamma = 1$ indicative of no interference. Moreover, CoC values close to 0 indicate high COI, whereas values close to 1 indicate absence of COI.

When fitting the frequency of inter-foci distances to a gamma distribution, we detected high γ values in all populations (from 9.5 to 16.2), accounting for the presence of COI. A detailed analysis of COI revealed further differences between populations (supplementary table S6, Supplementary Material online and Fig. 3e). St mice from the CFB^{St} population showed low centromere suppression, intermediate arm lengths (mean $7.6 \mu\text{m}$), and low levels of COI ($\gamma = 9.5$ and interference distance = 64% of bivalent arm), reflecting the high values of COs per cell detected in the cytology analysis (supplementary fig. S1B, Supplementary Material online). Remarkably, St mice from the CTR^{St} population presented the highest levels of CO interference ($\gamma = 16.2$ and interference distance = 72% of bivalent arm) and the lowest arm lengths (mean $7.5 \mu\text{m}$), explaining the low

number of arms with two foci detected that contribute to the reduced mean of COs per cell (Fig. 3b). Furthermore, CTRSt shows the lowest levels of centromere suppression, mirroring the analysis of the cumulative COs frequencies (Fig. 3c and d).

The presence of metacentric chromosomes and different bivalent configurations (i.e. acrocentric, homozygous, and heterozygous), increased the complexity of the patterns observed in Rb mice from the VDC^{Rb} population (supplementary fig. S1, E to I, Supplementary Material online). Despite the high mean values of arm length in VDC^{Rb} (7.86 μm) (which can result in high number of COs, Ruiz-Herrera et al. 2017), the presence of COI at the centromeric level (especially on metacentric chromosomes) (supplementary table S6, Supplementary Material online) resulted in a reduced proportion of chromosomal arms with two COs (Fig. 3b). These observations in combination with the mechanistic limitations of fusions and chromosomal configurations previously described (Vara et al. 2022) could explain the high percentage of chromosomal arms with zero COs and the reduction of mean values over the cell.

Multiple Genomic Landscapes of Recombination

We further estimated population-scaled RRs based on LD (see Materials and Methods). Broad-scale chromosome-specific recombination maps showed a high degree of variability between populations and chromosomes (Fig. 4). The St population CFBSt showed the highest level of RRs (mean values of 0.00122 ρ/bp), followed by CTRSt (mean values of 0.00075 ρ/bp) and then VDC^{Rb} (mean values of 0.0006 ρ/bp) (Wilcoxon pairwise test, P -value < 0.001, Fig. 5a). Both populations with reduced RRs genome-wide (CTRSt and VDC^{Rb}), showed more heterogeneous landscapes of recombination per chromosome. In contrast, CFBSt has higher values of RRs and showed a more homogeneous pattern genome-wide.

Interestingly, different landscapes of recombination were accompanied by contrasting patterns of broad hotspots distribution between populations. Both CTRSt and VDC^{Rb} populations (with heterogeneous landscapes of recombination) presented more than 400 broad hotspots distributed genome-wide, whereas its number was reduced by half in CFBSt (209 broad hotspots) (Fig. 5b). When analyzing the chromosomal distribution of broad hotspots considering proximal (from 0% to 14% of chromosome length), interstitial (from 14% to 80% of the chromosome), and distal (from 80% to 100% of chromosome length) regions, we detected significant differences (Chi-square test, P -value < 0.005) between populations (Fig. 5c), mirroring the cytological observations (Fig. 3). In CFBSt, the majority (79%) of broad hotspots were located in interstitial genomic regions, whereas in both CTRSt and VDC^{Rb} the distribution was more distally located (Fig. 5c).

When analyzing broad hotspots individually, we detected a low degree of overlap among populations (mean 33% of overlapping, Fig. 5d), reinforcing the presence of multiple genomic landscapes of recombination. The lowest degree

of overlap was detected between both St populations (CFBSt-CTRSt, 86 shared broad hotspots), whereas the populations that shared the allele 10A in homozygosis (CTRSt-VDC^{Rb}) showed the highest degree of coincidence (195 shared broad hotspots).

We next analyzed the broad hotspots overlapping between populations according to their genomic locations (again, in proximal, interstitial, or distal). When considering shared broad hotspots ($N = 195$) between populations with the same *Prdm9* alleles (CTRSt and VDC^{Rb} sharing the 10A allele) we detected that a high proportion (43%) were located at the distal regions with only few of them located in proximal chromosomal regions (4%) (Fig. 5d). This pattern (distribution toward telomeric regions) was also observed at the cytological level (Fig. 3). In contrast, shared broad hotspots ($N = 86$) between St populations with distinct *Prdm9* diversity (CFBSt and CTRSt) showed a more heterogeneous distribution across proximal (17%), interstitial (44%), and distal regions (39%).

The presence of multiple genomic landscapes of RRs was also reflected when analyzing the variation of recombination between populations. To do so, we estimated the variance to the mean ratio or index of dispersion (iod) and fitted it to a Poisson distribution to infer regions with an excess of variance (overdispersion, $R > 1$) across the genome. We detected the presence of 81 regions distributed across all chromosomes (21% of all 1 Mb genomic regions) with a variance between populations larger than expected (iod > 0.001) (supplementary fig. S2A, Supplementary Material online). These regions of high variability of RR between populations contained a total of 1,960 genes, distributed as protein-coding genes (42%), pseudogenes (29%), followed by noncoding RNAs (23%) (supplementary fig. S2B, Supplementary Material online). The remaining 6% corresponded to nonannotated transcripts. When analyzing the GO terms, we detected an enrichment (False Discovery Rate, FDR < 0.05 and Fold Enrichment, FE > 1.3) for genes related to the immune system (innate immune response, MHC class I protein complex, and T cell-mediated cytotoxicity) and nervous system (response to pheromone and sensory perception of smell) (supplementary fig. S2C, Supplementary Material online).

Moreover, we detected that estimated values of RRs were inversely correlated with genomic rates of differentiation. That is, St populations (CFBSt and CTRSt) showed low levels of genomic differentiation genome-wide (expressed as F_{ST} values), when compared to Rb mice (VDC^{Rb}) (Wilcoxon pairwise test, P -value < 0.001, Fig. 1e). A genomic scanning revealed the presence of 37 regions in the top 0.5% ranked windows which were candidates to be selective regions due to their highest F_{ST} value (supplementary fig. S3A, Supplementary Material online). A total of 634 transcripts were present in these regions, with a high percentage of them (41%) being protein-coding genes (supplementary fig. S3B, Supplementary Material online). GO analysis indicated that the protein-coding genes were associated with signaling pathways via JAK-STAT and G protein-coupled receptors, sensory

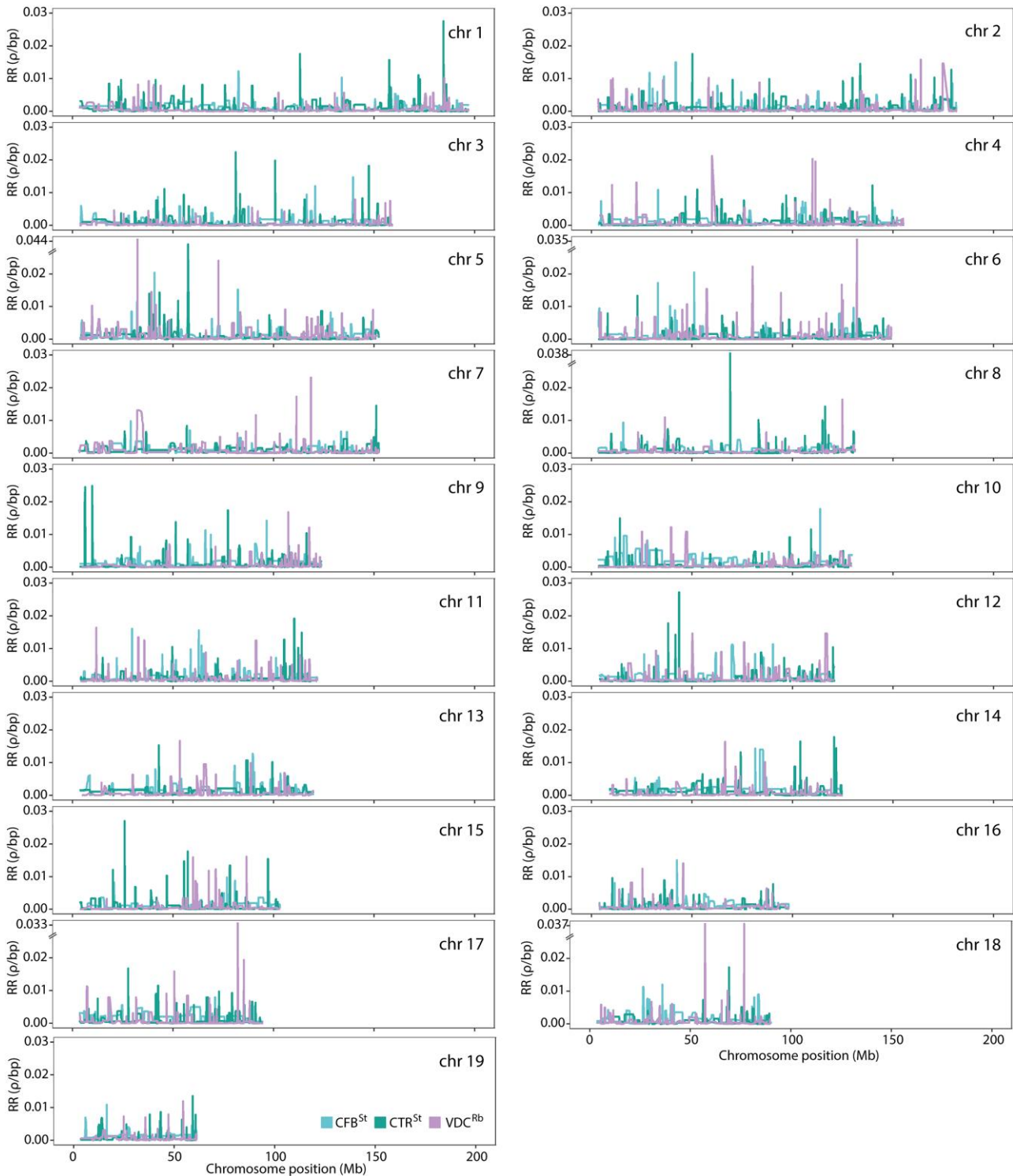


Fig. 4. Chromosome-specific recombination maps. Representation of estimated recombination rates (RR, units ρ/bp) per population and chromosome. Abbreviations: CFBSt, Castellfollit del Boix; CTRSt, Castellar del Vallès; VDC^{Rb}, Viladecans.

perception, cell population proliferation and response to nutrients, but also GO terms related to female reproduction (lactation, mammary gland development, and female pregnancy) (supplementary fig. S3C, Supplementary Material online). Importantly, sensory receptor genes included several olfactory protein families (Tas, Tcaf, and Olf).

Discussion

Our own study represents a departure from those conducted previously in that it relies on the use of genome-wide maps of RRs and genomic divergence in wild populations of mice with Rb fusions in combination with *Prdm9* sequencing.

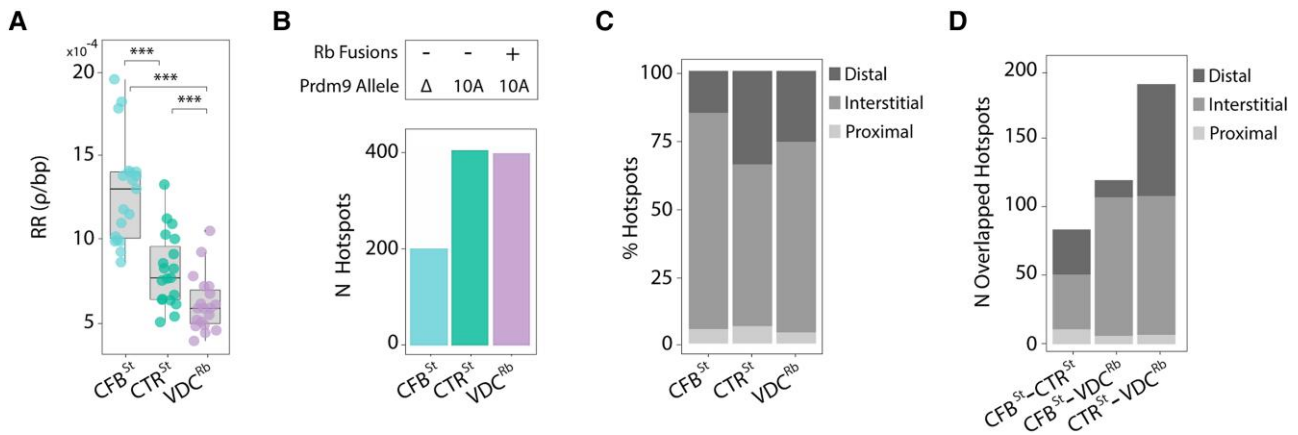


Fig. 5. Estimates of RR and distribution of recombination broad hotspots. a) Genome-wide levels of RR (ρ /bp) per population with dots representing different chromosomes. Wilcoxon pairwise test ($***P < 0.001$). b) Number of broad hotspots detected in each population. Information relative to the presence of Rb fusions and *Prdm9* allelic background per population is included in the upper panel. c) Distribution of broad hotspots along three genomic fractions: proximal (0% to 14% of chromosomal length), interstitial (14% to 80% of chromosomal length), and distal (80% to 100% of chromosomal length). d) Number and distribution of broad hotspots overlapping between populations. Abbreviations: CFBSt, Castellfollit del Boix; CTRSt, Castellar del Vallès; VDC^{Rb}, Viladecans; St, standard mice; Rb, Robertsonian.

Using an integrative approach that combined estimates of RRs based on SNP genotyping and cytological analysis of meiotic COs on male germ cells, here we show that chromosomal fusions and *Prdm9* allelic background can affect meiotic recombination in natural populations of house mice, resulting in a combined impact at the genomic level (Fig. 6).

Chromosomal Fusions as Modifiers of Meiotic Recombination

Using both direct (immunolocalization of meiotic COs) and indirect (LD and genomic divergence) measures of recombination we detected that the presence of Rb fusions was associated with reduced levels of recombination. A detailed cytological analysis revealed that the reduction in CO numbers can be influenced by the presence of fused chromosomes in homozygous state, concomitant with the presence of bivalents with misaligned centromeres previously described in the literature (Vara et al. 2021).

The observed reduction of COs in homozygous fused chromosomes was associated with a suppression of recombination in centromeric regions, resulting in a displacement of COs toward telomeric regions of the chromosome (Fig. 6). According to the “suppressed recombination” model (Rieseberg 2001; Faria and Navarro 2010; Farré et al. 2013), a reduction in recombination rate is expected within reorganized regions in heterokaryotypes. Here, however, we showed that acrocentric and fused chromosomes in homozygous state were also affected by a reduction of COs and that this variation was associated with changes in COI.

Despite possible biological cofounds, previous studies on wild-derived mice with Rb fusions have shown a significant decrease in chiasmata frequencies and meiotic COs (Bidau et al. 2001; Castiglia and Capanna 2002; Dumas and Britton-Davidian 2002; Manterola et al. 2009; Vasco et al. 2012; Capilla et al. 2014). Therefore, evidence suggest

that despite the presence of any genetic heterogeneity, Rb fusions can introduce strong mechanistic constraints inside the nucleus of meiocytes that can result in a displacement of COs along chromosomal axis, affecting asynapsis in prophase I (Manterola et al. 2009; Ribagorda et al. 2019). This structural effect has also been shown when analyzing the 3D genome structure, detecting that fusions alter the nuclear architecture during meiosis, including an increased rate of heterologous interactions in primary spermatocytes, and alterations in both chromosome synapsis and axis length (Vara et al. 2021).

In the case of natural Rb populations, where the distribution of metacentric chromosomes is widespread (Pialek et al. 2005), the presence of heterokaryotypes with a high number of Rb fusions is not expected to be common. In fact, the prevalence of Rb fusions in heterozygous state was moderate in BRbS (from one to three trivalents). This phenomenon is probably related to a negative selection for heterokaryotypes (underdominance) (Dobigny et al. 2017 and references therein). That is, the lower the degree of underdominance associated with a particular Rb fusion, the higher the probability to be present as a polymorphic form. Thus, the presence of Rb fusions in the BRbS can be related to a mild underdominance, given that previous studies in this system did not detect strong fertility impairment (Sans-Fuentes et al. 2010; Medarde et al. 2015). Despite a chromosomal redistribution and reduction of COs in Rb mice, the frequency of chromosomal arms with absence of COs was not significantly altered in mice with Rb fusions in heterozygosis. This observation has important implications since it suggests that meiosis is not severely compromised in Rb mice from the BRbS, given that the proper disjunction of chromosomes would not be compromised as at least one CO is present per bivalent (Hassold et al. 2000; Segura et al. 2013). This is consistent with mild effects in reproduction previously reported in

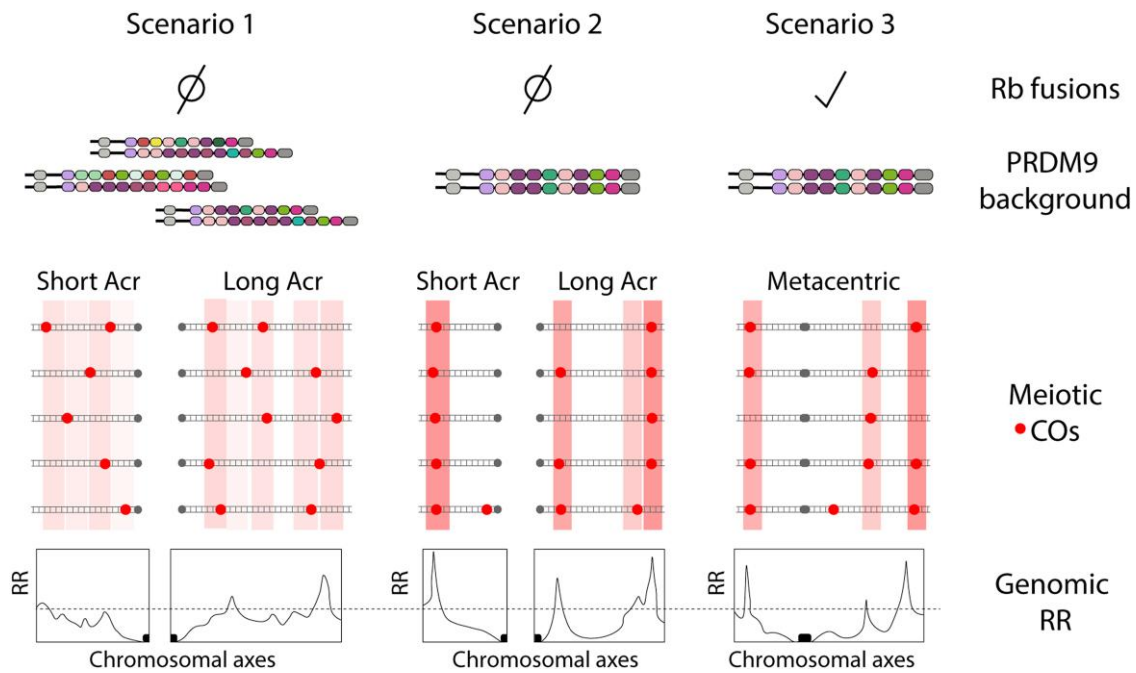


Fig. 6. Proposed model for the existence of different genomic landscapes of recombination in wild populations carrying Rb fusions in the presence of different *Prdm9* allelic backgrounds. The first scenario includes standard mice (absence of Rb fusions) with different *Prdm9* alleles (mainly heterozygous). In this case, meiotic COs are distributed along chromosomes since there is competition between the *Prdm9* alleles and no structural restrictions due to the Rb fusions. This pattern results in high rates of recombination genome-wide, both at the cytological and population level, but with few local regions of high recombination rate (hence, broad hotspots). The second scenario includes standard mice (absence of Rb fusions) with the *Prdm9* allele in homozygosis. In this case the placement of COs is more stable between meicyotes and individuals, resulting in high numbers of broad hotspots of recombination at the population level. The third scenario represents Rb mice (metacentric chromosomes) with the same *Prdm9* allele in homozygosis. Here there is a reduction and redistribution of COs toward telomeric regions. This also results in high numbers of broad hotspots of recombination at the population level. Abbreviations: COs, crossovers; RR, recombination rates.

different *M. m. domesticus* Rb systems with one to three fusions (Wallace et al. 1992, 2002; Castiglia and Capanna 2000). Under this scenario, a reduction of recombination due to the presence of a relatively low number of Rb fusions present as chromosomal polymorphism does not necessarily affect fertility significantly but can lead to an increase in genetic divergence genome-wide.

Importantly, comparisons of recombination rate divergence between BRbS populations suggest that genomic landscapes recombination evolves very rapidly, accelerated by the presence of Rb fusions in the context of wild populations. Importantly, and consistent with the observation of low CO frequencies (MLH1 foci per cell) and low values of genome-wide RRs (expressed as ρ /bp), Rb mice showed higher levels of genomic divergence. Together with heterozygous mild underdominance, the effect of Rb fusions could lead to the accumulation of genetic incompatibilities and possibly to genetic isolation between populations, as has been suggested in other systems (Noor et al. 2001; Rieseberg 2001; Faria and Navarro 2010). Importantly, scans for genomic regions with high levels of differentiation in populations from the BRbS pointed to multiple candidate genes and pathways for metabolic processes, olfactory receptor signaling and female reproduction. We have previously suggested that Rb fusions can redistribute chromosomal nuclear occupancy in spermatocytes,

exposing chromosomal domains to novel regulatory environments, potentially affecting gene expression and/or regulation (Vara et al. 2021). This is especially relevant for olfactory receptor family clusters detected in the present study (Tas, Tcaf, and Olf gene families), which can be expressed in the germ line and being involved in reproduction. We can anticipate that altered regulation of their expression could play an adaptive role in the BRbS. Further studies will be needed to validate this hypothesis.

Combined Effect of *Prdm9* Allelic Background and Rb Fusions in Reshaping Genomic Landscapes of Recombination

As recombination hotspots in mammals are mainly determined by PRDM9, we sought to investigate the contribution of the allelic variability of *Prdm9* to genomic landscapes of recombination in wild populations. Previous studies conducted in the BRbS (Vara et al. 2019, 2021) already showed that trends broadly hold across multiple Rb and St populations, providing an extensive survey of *Prdm9* diversity and patterns of CO distribution in Rb systems. The present analysis unveils new contrasting patterns of *Prdm9* variability in St populations. On the one hand, we add new alleles to previous surveys (Buard et al. 2014; Capilla et al. 2014; Kono et al. 2014; Vara

et al. 2019). On the other hand, we detect one St population (CTRSt) that was mainly homozygous for the 10A allele, which was present in all populations, but especially in Rb mice. This permits the opportunity to compare (despite genetic divergence) populations with different set of attributes (Fig. 6): (i) populations homogeneous in their chromosome complement (no Rb fusions) but different *Prdm9* allelic composition (e.g. CFBSt vs. CTRSt); and (ii) populations homozygous for *Prdm9* but with different chromosome complement (e.g. CTRSt vs. VDC^{Rb}).

Interestingly, the presence of the 10A *Prdm9* allele in CTRSt could be explained as the result of a population bottleneck event that facilitated the formation and subsequent expansion of new populations. According to the PCA and ancestry analysis, St mice populations such as CFBSt, represent the origin of the genetic diversity from where populations such as CTRSt and Rb mice populations diverged. The genetic divergence detected in the BRbS can be due to a combination of different factors, including the geographical distribution of populations, as previously suggested (Medarde et al. 2012), but also by the presence of metacentric chromosomes that can lead to a reduction of gene flow. Moreover, the phylogenetic relationships among populations suggest that the BRbS may represent an example of radiation and independent origin of Rb fusions occurring in nature. Further studies will be needed to elucidate the mechanisms of Rb fusions formation in wild populations.

However, regardless the evolutionary origin of wild mice population, distinctive patterns of *Prdm9* allelic background allowed us to explore the functional constraints that might influence recombination in the presence of Rb fusions. It has been described that the presence of highly divergent *Prdm9* alleles in a heterozygous state (as in the case of the St population CFBSt) can lead to elevated levels of asymmetric DSBs between homologous chromosomes (Davies et al. 2016). In fact, evidence in humans and mice has shown that variation in both the sequence and number of ZnF repeats influence the distribution of meiotic DSBs (Berg et al. 2010; Brick et al. 2012; Baker et al. 2015; Grey et al. 2018). The rapid evolution of ZnF sequences would therefore lead to rapid changes in the distribution of recombination sites across the genome by creating new DNA motifs that would be recognized with stronger affinity by the new *Prdm9* allelic variants. This is what we observed in St mice from the CFBSt (a population with a high *Prdm9* allelic diversity), which showed higher levels of RRs genome wide but lower number of broad hotspots when compared to CTRSt and VDC^{Rb} (both populations homozygous for the 10A allele). Therefore, the low number of broad-scale hotspots at population level detected in CFBSt could be related with the high diversity of *Prdm9* and the consequent low intensity of recombination in genomic regions (Fig. 6). Conversely, *Prdm9* alleles in a homozygous state (as the 10A allele in CTRSt and VDC^{Rb} populations) can produce symmetric DSBs between homologous chromosomes, hence low numbers of COs. This effect, in combination with an increase in COI resulted in

low levels of RRs genome-wide but high number of broad hotspots (Fig. 6). Consistently with this view, previous studies of RAD51 foci (marker of meiotic DSBs) in spermatocytes from the VDC^{Rb} population (Vara et al. 2021) detected low levels of DSBs in Rb mice when compared to St wild mice, suggesting that *Prdm9* homozygosity produce symmetric hotspots.

Overall, our results showed that of Rb fusions can have genomic implications. The presence of Rb fusions can result in a redistribution of meiotic COs across chromosomes, thus reducing RR genome-wide. Importantly, this redistribution of recombination can affect not only chromosomes involved in Rb fusions but also nonfused chromosomes, resulting in higher levels of genetic differentiation genome-wide. This was especially relevant for genomic regions with high levels of divergence containing genes relevant for reproduction.

Materials and Methods

Mice Sampling

A total of 108 house mice (*M. m. domesticus*) from the BRbS were included in the study (Fig. 1 and supplementary table S1, Supplementary Material online). These represented five wild populations: two populations of mice with a St karyotype ($2n = 40$) (CFBSt, $N = 29$; CTRSt, $N = 23$), and three populations of mice with Rb fusions (thereafter Rb mice) with a variable number of Rb fusions ($2n = 39$ to 28) (CS^{Rb}, $N = 15$; SS^{Rb}, $N = 12$; VDC^{Rb}, $N = 29$). Animals were treated and processed in accordance with ethical guidelines approved by the Universitat Autònoma de Barcelona.

SNP Genotyping and Genome Diversity

Genomic DNA was extracted either from tissue biopsies preserved in ethanol or fresh tissue using a standard proteinase K digestion protocol (Vara et al. 2019). The genotyping data included 55 mice from five populations (supplementary table S1, Supplementary Material online). Briefly, 31 mice were genotyped using the Mega Mouse Universal Genotyping Array (MegaMUGA, including 77,808 SNPs, data retrieved from Vara et al. 2019) whereas 24 mice were newly genotyped using GigaMUGA array (143,259 SNPs) (Morgan and Welsh 2015; Morgan et al. 2016). SNPs data from both MUGA arrays were merged. The resulting SNP dataset was filtered with missing values above the 5% threshold and Hardy–Weinberg equilibrium exact test below 1×10^{-5} , yielding a final dataset of 47,200 informative SNPs evenly distributed across the genome with a mean density of 1 SNP each 58 kb. Based on this dataset, genetic differentiation among individuals was inferred using principal component analysis (PCA) running a module of PLINK 1.9 (Chang et al. 2015). Parallely, the genetic structure among populations and individual ancestry was evaluated using ADMIXTURE 1.3.0 (Alexander et al. 2009). Moreover, we inferred evolutionary relationships between populations generating a maximum

likelihood tree with SNPhylo (Lee et al. 2014). Summary statistics related to genetic diversity were calculated, including the number of alleles (Na), allelic richness (Ar), observed heterozygosity (H_o), expected heterozygosity (H_e), inbreeding coefficient (Fis), and nucleotide diversity (π). Na and Ar were estimated using Hierfstat v0.5-11 (Goudet 2005) implemented in R. H_o , H_e , and Fis were calculated using the module-het of PLINK v1.9, and pi with VCFtools 0.1.15 (Danecek et al. 2011).

Amplification of the ZnF Array of *Prdm9*

The ZnF array of the *Prdm9* gene is encoded by the last exon (exon 12) and it extends from the first ZnF repeat toward the C-terminal domain (Parvanov et al. 2010). We amplified this last exon as previously described (Kono et al. 2014; Vara et al. 2019). This served to identify homozygous and heterozygous mice. Once heterozygous mice were detected, allelic-specific amplification was generated using the band-stab PCR protocol (Bjourson and Cooper 1992). Briefly, this included two identical PCR cycles: 94 °C (5'), 30 cycles of 94 °C (40"), 68 °C (50"), and 72 °C (60"), followed by 72 °C (3'). A unique PCR round was used for homozygous mice with the same PCR conditions. All PCR products were purified with EXOSAP and sequenced. *Prdm9* alleles were classified according to the number of ZnF repeats (and therefore the size of the sequence) and the amino acids present in the hypervariable positions -1, +3, and +6 of the first ZnF repeats (ZnF3, ZnF4, ZnF5, and ZnF6), as previously described (Vara et al. 2019).

Summary population genetics metrics and selection tests were computed using DnaSP v.6.12.03 (Rozas et al. 2017) for each population separately, with sequences aligned against the rat reference *Prdm9* coding sequence as obtained from Genbank (NM_001108903.2) (Sayers et al. 2023). Only the sequence of the ZnF repeats 3 to 10 was considered, including 84 nucleotide sites (28 codons) for each repeat, or 672 nucleotide sites (224 codons) in total. Due to missing nucleotides in some sequences at the alignment ends, a total of 563 nucleotide sites were analyzed in the CFBSt population and 670 nucleotide sites in all other four populations. The summary metrics and selection tests computed include nucleotide diversity (π) (Nei 1987), π_a/π_s (Nei and Gojobori 1986), Fu-Li's D (Fu and Li, 1993), Tajima's D (Tajima 1989), and McDonald-Kreitman test (McDonald and Kreitman 1991) with the corresponding NI (Rand and Kann 1996).

For the sliding windows analyses, the size of the windows considered was 3 nucleotide sites, with a step of 3 nucleotide sites, including sites with alignment gaps; thus, all metrics and selection tests were computed for each codon separately. Then, we classified the observed number of segregating nucleotide sites as falling within the hypervariable positions (-1, +3, and +6), or outside them. We further computed the corresponding expected values by randomly distributing the observed numbers among both categories of nucleotide sites according to their proportions in the sequence (out of 84 nucleotide

sites in each ZnF, 9 correspond to hypervariable positions -1, +3, and +6, and 75 do not). By putting together observed and expected values, we computed a 2 × 2 contingency table and tested its significance with a Fisher's Exact Goodness-of-fit test for each ZnF separately, and ZnF3 to ZnF6 altogether.

Spermatocyte Spreads and Immunofluorescence

Spermatocyte spreads were performed as previously reported (García-Cruz et al. 2011; Capilla et al. 2014; Marín-Gual et al. 2022). Immunostaining of meiocytes was performed using the following primary antibodies: rabbit antibody against SYCP3 (#ab15093, Abcam, 1:400 dilution), mouse antibody against MLH1 (#ab14206, Abcam, 1:50 dilution), human calcinosis, Raynaud's phenomenon, esophageal dysfunction, sclerodactyly and telangiectasia (CREST) serum (a kind gift of M. Fritzler, 1:100 dilution). Fluorochrome-conjugated secondary antibodies were used for detection (all from Jackson ImmunoResearch Laboratories, 1:200 dilution). The immunostaining protocol included antigen retrieval with incubation in sodium citrate buffer (10 mM sodium citrate, 0.05% Tween-20; pH 6.0) at 95 °C for 15 min and permeabilization steps with PBST (0.05% Triton X-100 in PBS), and overnight incubation for primary antibodies at 4 °C and 1 h for secondary at 37 °C, both in a humidified chamber.

Cytological Analysis of COs

Images were analyzed using an epifluorescence microscope (Axiophot, Zeiss) equipped with suitable emission filters (DAPI, FITC, Cy3, and Cy5). Images were captured using ACO XY program (A. Coloma, Open Microscopy) and stacked using Adobe Photoshop 7.0. Only meiocytes at the pachytene stage were included for the cytological analysis of COs. Total numbers of COs per cell and per bivalent arm were scored. Bivalent length measures and the relative position of COs (accounted as a percentage of the total synaptonemal complex length from centromere to telomere) were performed with Micromerasure 3.3 (Reeves 2001) as previously described (Segura et al. 2013; Ruiz-Herrera et al. 2017; Vara et al. 2021).

CO interference (COI) was measured by analyzing the CoC using MADpattern v1.1 (Jones and Franklin 2006; White et al. 2017; Wang et al. 2019). Each chromosomal arm was normalized to 100% of total length and divided into 20 intervals for CO scoring. For each pair of intervals, the experimentally observed frequency of double COs (arms with a CO in both intervals) was compared to the expected frequency (the product of the frequencies of observed COs in each interval alone). The ratio of observed to expected double COs (CoC) was plotted as a function of the normalized inter-interval distance.

Estimates of Recombination Rates

Estimates of RR based on LD were conducted in a subset of 24 mice genotyped with GigaMUGA, excluding the sex chromosomes (X and Y) (supplementary table S1,

Supplementary Material online). Samples were selected based on SNP density (1 SNPs per 50 kb) and *Prdm9* genetic background. This included mice from three wild-mice populations: CFBSt ($N = 7$), CTRSt ($N = 6$), and VDC^{Rb} ($N = 11$). SNPs were filtered with missing values above the 5% threshold and Hardy–Weinberg equilibrium exact test below 1×10^5 . SNPs data was phased with SHAPEIT (Delaneau et al. 2012) to obtain population haplotypes. Likelihood tables were generated with Ldpop (Alexander and Machiela 2020). Then, Ldhelmet (Chan et al. 2012) was used to estimate the population-scaled RR for each chromosome using default parameters as previously described (Vara et al. 2021).

Given SNP density (~1 SNP every 50 kb), inferences of RR were determined at intermediate genomic scales (~1 Mb). Genomic regions with high values of RRs were identified comparing the ρ value of recombination of each SNP with the mean ρ of the 1 Mb flanking region. Those 1 Mb regions with a comparative value higher than 5 were considered “broad hotspots”. Moreover, the variance of RRs per genomic region between populations was also estimated as the variance to mean ratio (iod) (Gillespie 1989; Comeron et al. 2012), considering nonoverlapping 1 Mb windows. Under a Poisson distribution, iod values significantly greater than 1 indicate an excess of variance and are considered regions of high variance between populations.

Lastly, genetic divergence between populations was calculated by computing Weir and Cockerham’s F_{ST} values (Hudson et al. 1992) using VCFtools 0.1.15 (Danecek et al. 2011). F_{ST} analysis was conducted between populations considering nonoverlapping 1 Mb genomic windows at two levels: per chromosome and genome-wide.

GO Analysis

Gene ontology (GO) analyses were performed using PANTHER db (Thomas et al. 2003). Statistical overrepresentation test was selected with GO biological process complete. Only GO terms with $FE \geq 1.3$ and $FDR < 0.05$ were considered statistically significant.

Supplementary Material

Supplementary material is available at *Molecular Biology and Evolution* online.

Acknowledgments

This work was supported by the Ministry of Economy, Industry and Competitiveness (CGL2017-83802-P to A.R.-H.), the Spanish Ministry of Science and Innovation (PID2020-112557GB-I00/AEI/10.13039/501100011033 to A.R.-H.), the Agència de Gestió d’Ajuts Universitaris i de Recerca, AGAUR (2021SGR00122 to A.R.-H.). C.M.-G. was supported by a PIF predoctoral fellowship from the Universitat Autònoma of Barcelona (2020/D/LE/CC/3). C.V. and L.A.-G. were supported by FPI predoctoral fellowships from the Ministry of Economy and Competitiveness (BES-2015-072924 and PRE-2018-083257, respectively). L.M.-G. was supported by an FPU predoctoral fellowship

from the Ministry of Science, Innovation and University (FPU18/03867).

Author Contributions

C.M.-G. and A.R.-H. designed experiments. C.M.-G., L.M.-G., J.P., M.M.G.-R., and C.V. performed experiments. C.M.-G., L.A.-G., S.C., J.P., and K.Y. analyzed the data. J.V. and A.R.-H. contributed to reagents and data collection. C.M.-G. and A.R.-H. wrote the initial draft of the manuscript with inputs from all authors. All authors provided comments and gave final approval for publication.

Data Availability

The SNP data are available at GEO repository with ID GSE254746.

References

- Alexander TA, Machiela MJ. LDpop: an interactive online tool to calculate and visualize geographic LD patterns. *BMC Bioinformatics*. 2020;**21**(1):1–4. <https://doi.org/10.1186/s12859-020-3340-1>.
- Alexander DH, Novembre J, Lange K. Fast model-based estimation of ancestry in unrelated individuals. *Genome Res*. 2009;**19**(9):1655–1664. <https://doi.org/10.1101/gr.094052.109>.
- Álvarez-González L, Arias-Sardá C, Montes-Espuña L, Marín-Gual L, Vara C, Lister NC, Cuartero Y, García F, Deakin J, Renfree MB, et al. Principles of 3D chromosome folding and evolutionary genome reshuffling in mammals. *Cell Rep*. 2022a;**41**:12. <https://doi.org/10.1016/j.celrep.2022.111839>.
- Álvarez-González L, Burden F, Doddamani D, Malinverni R, Leach E, Marín-García C, Marín-Gual L, Gubern A, Vara C, Paytuvi-Gallart A, et al. 3D chromatin remodelling in the germ line modulates genome evolutionary plasticity. *Nat Commun*. 2022b;**13**(1):1–15. <https://doi.org/10.1038/s41467-022-30296-6>.
- Baker CL, Petkova P, Walker M, Flachs P, Mihola O, Trachtulec Z, Petkov PM, Paigen K. Multimer formation explains allelic suppression of PRDM9 recombination hotspots. *PLoS Genet*. 2015;**11**(9):1–24. <https://doi.org/10.1371/journal.pgen.1005512>.
- Baudat F, Buard J, Grey C, Fledel-Alon A, Ober C, Przeworski M, Coop G, de Massy B. PRDM9 is a major determinant of meiotic recombination hotspots in humans and mice. *Science*. 2010;**327**(5967):836–840. <https://doi.org/10.1126/science.1183439>.
- Berg IL, Neumann R, Lam KWG, Sarbajna S, Odenthal-Hesse L, May CA, Jeffreys AJ. PRDM9 variation strongly influences recombination hot-spot activity and meiotic instability in humans. *Nat Genet*. 2010;**42**(10):859–863. <https://doi.org/10.1038/ng.658>.
- Berg IL, Neumann R, Sarbajna S, Odenthal-Hesse L, Butler NJ, Jeffreys AJ. Variants of the protein PRDM9 differentially regulate a set of human meiotic recombination hotspots highly active in African populations. *Proc Natl Acad Sci USA*. 2011;**108**(30):12378–12383. <https://doi.org/10.1073/pnas.1109531108>.
- Bidau CJ, Giménez MD, Palmer CL, Searle JB. The effects of Robertsonian fusions on chiasma frequency and distribution in the house mouse (*Mus musculus domesticus*) from a hybrid zone in northern Scotland. *Heredity*. 2001;**87**(3):305–313. <https://doi.org/10.1046/j.1365-2540.2001.00877.x>.
- Billings T, Parvanov ED, Baker CL, Walker M, Paigen K. DNA binding specificities of the long zinc-finger recombination protein PRDM9. *Genome Biol*. 2013;**14**(4):R35. <https://doi.org/10.1186/gb-2013-14-4-r35>.

- Bjourson AJ, Cooper JE. Band-stab PCR: a simple technique for the purification of individual PCR products. *Nucleic Acids Res.* 1992;**20**(17):4675. <https://doi.org/10.1093/nar/20.17.4675>.
- Brick K, Smagulova F, Khil P, Camerini-Otero RD, Petukhova GV. Genetic recombination is directed away from functional genomic elements in mice. *Nature.* 2012;**485**(7400):642–645. <https://doi.org/10.1038/nature11089>.
- Buard J, Rivals E, Dunoyer De Segonzac D, Garres C, Caminade P, De Massy B, & Boursot P. Diversity of *Prdm9* zinc finger array in wild mice unravels new facets of the evolutionary turnover of this coding minisatellite. *PLoS ONE.* 2014;**9**(1):e85021. <https://doi.org/10.1371/journal.pone.0085021>.
- Capilla L, Medarde N, Alemany-Schmidt A, Oliver-Bonet M, Ventura J, Ruiz-Herrera A. Genetic recombination variation in wild Robertsonian mice: on the role of chromosomal fusions and *Prdm9* allelic background. *Proc R Soc B Biol Sci.* 2014;**281**:20140297. <https://doi.org/10.1098/rspb.2014.0297>.
- Castiglia R, Capanna E. Contact zone between chromosomal races of *Mus musculus domesticus*. 2. Fertility and segregation in laboratory-reared and wild mice heterozygous for multiple Robertsonian rearrangements. *Heredity.* 2000;**85**(2):147–156. <https://doi.org/10.1046/j.1365-2540.2000.00743.x>.
- Castiglia R, Capanna E. Chiasma repatterning across a chromosomal hybrid zone between chromosomal races of *Mus musculus domesticus*. *Genetica.* 2002;**114**(1):35–40. <https://doi.org/10.1023/A:1014626330022>.
- Chan AH, Jenkins PA, Song YS. Genome-wide fine-scale recombination rate variation in *Drosophila melanogaster*. *PLoS Genet.* 2012;**8**(12):e1003090. <https://doi.org/10.1371/journal.pgen.1003090>.
- Chang CC, Chow CC, Tellier LCAM, Vattikuti S, Purcell SM, Lee JJ. Second-generation PLINK: rising to the challenge of larger and richer datasets. *GigaScience.* 2015;**4**(1):1–16. <https://doi.org/10.1186/s13742-015-0047-8>.
- Comeron JM, Ratnappan R, Bailin S. The many landscapes of recombination in *Drosophila melanogaster*. *PLoS Genet.* 2012;**8**(10):33–35. <https://doi.org/10.1371/journal.pgen.1002905>.
- Danecek P, Auton A, Abecasis G, Albers CA, Banks E, DePristo MA, Handsaker RE, Lunter G, Marth GT, Sherry ST, et al. The variant call format and VCFtools. *Bioinformatics.* 2011;**27**(15):2156–2158. <https://doi.org/10.1093/bioinformatics/btr330>.
- Davies B, Hatton E, Altemose N, Hussin JG, Pratto F, Zhang G, Hinch AG, Moralli D, Biggs D, Diaz R, et al. Re-engineering the zinc fingers of PRDM9 reverses hybrid sterility in mice. *Nature.* 2016;**530**(7589):171–176. <https://doi.org/10.1038/nature16931>.
- Delaneau O, Marchini J, Zagury JF. A linear complexity phasing method for thousands of genomes. *Nat Methods.* 2012;**9**(2):179–181. <https://doi.org/10.1038/nmeth.1785>.
- Diagouraga B, Clément JA, Duret L, Kadlec J, de Massy B, Baudat F. PRDM9 methyltransferase activity is essential for meiotic DNA double-strand break formation at its binding sites. *Mol Cell.* 2018;**69**(5):853–865. <https://doi.org/10.1016/j.molcel.2018.01.033>.
- Dobigny G, Britton-Davidian J, Robinson TJ. Chromosomal polymorphism in mammals: an evolutionary perspective. *Biol Rev.* 2017;**92**(1):1–21. <https://doi.org/10.1111/brv.12213>.
- Dumas D, Britton-Davidian J. Chromosomal rearrangements and evolution of recombination: comparison of chiasma distribution patterns in standard and Robertsonian populations of the house mouse. *Genetics.* 2002;**162**(3):1355–1366. <https://doi.org/10.1093/genetics/162.3.1355>.
- Faria R, Navarro A. Chromosomal speciation revisited: rearranging theory with pieces of evidence. *Trends Ecol Evol.* 2010;**25**(11):660–669. <https://doi.org/10.1016/j.tree.2010.07.008>.
- Farré M, Micheletti D, Ruiz-Herrera A. Recombination rates and genomic shuffling in human and chimpanzee—a new twist in the chromosomal speciation theory. *Mol Biol Evol.* 2013;**30**(4):853–864. <https://doi.org/10.1093/molbev/mss272>.
- Förster DW, Mathias ML, Britton-Davidian J, Searle JB. Origin of the chromosomal radiation of Madeiran house mice: a microsatellite analysis of metacentric chromosomes. *Heredity.* 2013;**110**(4):380–388. <https://doi.org/10.1038/hdy.2012.107>.
- Franchini P, Colangelo P, Solano E, Capanna E, Verheyen E, Castiglia R. Reduced gene flow at pericentromeric loci in a hybrid zone involving chromosomal races of the house mouse *Mus musculus domesticus*. *Evolution.* 2010;**64**(7):2020–2032. <https://doi.org/10.1111/j.1558-5646.2010.00964.x>.
- Fu YX, Li WH. Statistical tests of neutrality of mutations. *Genetics.* 1993;**133**(3):693–709. <https://doi.org/10.1093/genetics/133.3.693>.
- García-Cruz R, Pacheco S, Briño MA, Steinberg ER, Mudry MD, Ruiz-Herrera A, García-Caldés M. A comparative study of the recombination pattern in three species of Platyrrhini monkeys (Primates). *Chromosoma.* 2011;**120**(5):521–530. <https://doi.org/10.1007/s00412-011-0329-6>.
- Gergelits V, Parvanov E, Simecek P, Forejt J. Chromosome-wide characterization of meiotic noncrossovers (gene conversions) in mouse hybrids. *Genetics.* 2021;**217**(1):1–14. <https://doi.org/10.1093/genetics/iyaa013>.
- Gillespie JH. Lineage effects and the index of dispersion of molecular evolution. *Mol Biol Evol.* 1989;**6**(6):636–647. <https://doi.org/10.1093/oxfordjournals.molbev.a040576>.
- Girard C, Zwicker D, Mercier R. The regulation of meiotic crossover distribution: a coarse solution to a century-old mystery? *Biochem Soc Trans.* 2023;**0**:1–12. <https://doi.org/10.1042/BST20221329>.
- Goudet J. HIERFSTAT, a package for R to compute and test hierarchical F-statistics. *Mol Ecol Notes.* 2005;**5**(1):184–186. <https://doi.org/10.1111/j.1471-8286.2004.00828.x>.
- Gregorova S, Gergelits V, Chvatalova I, Bhattacharyya T, Valiskova B, Fotopulosova V, Jansa P, Wiatrowska D, Forejt J. Modulation of *Prdm9*-controlled meiotic chromosome asynapsis overrides hybrid sterility in mice. *ELife.* 2018;**7**:e34282. <https://doi.org/10.7554/eLife.34282>.
- Grey C, Baudat F, de Massy B. *Prdm9*, a driver of the genetic map. *PLoS Genet.* 2018;**14**(8):1–24. <https://doi.org/10.1371/JOURNAL.PGEN.1007479>.
- Groeneveld LF, Atencia R, Garriga RM, Vigilant L. High diversity at PRDM9 in chimpanzees and bonobos. *PLoS ONE.* 2012;**7**(7):24–26. <https://doi.org/10.1371/journal.pone.0039064>.
- Guerrero RF, Kirkpatrick M. Local adaptation and the evolution of chromosome fusions. *Evolution.* 2014;**68**(10):2747–2756. <https://doi.org/10.1111/evo.12481>.
- Gündüz I, López-Fuster MJ, Ventura J, Searle JB. Clinal analysis of a chromosomal hybrid zone in the house mouse. *Genet Res.* 2001;**77**(1):41–51. <https://doi.org/10.1017/S0016672300004808>.
- Hassold T, Sherman S, Hunt P. Counting cross-overs: characterizing meiotic recombination in mammals. *Hum Mol Genet.* 2000;**9**(16):2409–2419. <https://doi.org/10.1093/hmg/9.16.2409>.
- Hudson RR, Slatkin M, Maddison WP. Estimation of levels of gene flow from DNA sequence data. *Genetics.* 1992;**132**(2):583–589. <https://doi.org/10.1093/genetics/132.2.583>.
- Jones GH, Franklin FCH. Meiotic crossing-over: obligation and interference. *Cell.* 2006;**126**(2):246–248. <https://doi.org/10.1016/j.cell.2006.07.010>.
- Keeney S, Giroux CN, Kleckner N. Meiosis-specific DNA double-strand breaks are catalyzed by Spo11, a member of a widely conserved protein family. *Cell.* 1997;**88**(3):375–384. [https://doi.org/10.1016/S0092-8674\(00\)81876-0](https://doi.org/10.1016/S0092-8674(00)81876-0).
- King M. *Species evolution: the role of chromosome change*. Cambridge: Cambridge University Press; 1995.
- Kirkpatrick M. How and why chromosome inversions evolve. *PLoS Biol.* 2010;**8**(9):e1000501. <https://doi.org/10.1371/journal.pbio.1000501>.
- Kono H, Tamura M, Osada N, Suzuki H, Abe K, Moriwaki K, Ohta K, Shiroishi T. *Prdm9* polymorphism unveils mouse evolutionary tracks. *DNA Res.* 2014;**21**(3):315–326. <https://doi.org/10.1093/dnares/dst059>.
- Lee TH, Guo H, Wang X, Kim C, Paterson AH. SNPPhylo: a pipeline to construct a phylogenetic tree from huge SNP data. *BMC*

- Genomics*. 2014;**15**(1):1–6. <https://doi.org/10.1186/1471-2164-15-162>.
- Li R, Bitoun E, Altemose N, Davies RW, Davies B, Myers SR. A high-resolution map of non-crossover events reveals impacts of genetic diversity on mammalian meiotic recombination. *Nat Commun*. 2019;**10**(1):24–29. <https://doi.org/10.1038/s41467-019-11675-y>.
- Mackintosh A, Vila R, Laetsch DR, Hayward A, Martin SH, Lohse K. Chromosome fissions and fusions act as barriers to gene flow between *Brenthis fritillaria* butterflies. *Mol Biol Evol*. 2023;**40**(3): 1–13. <https://doi.org/10.1093/molbev/msad043>.
- Manterola M, Page J, Vasco C, Berríos S, Parra MT, Viera A, Rufas JS, Zuccotti M, Garagna S, Fernández-Donoso R. A high incidence of meiotic silencing of unsynapsed chromatin is not associated with substantial pachytene loss in heterozygous male mice carrying multiple simple Robertsonian translocations. *PLoS Genet*. 2009;**5**(8): e1000625. <https://doi.org/10.1371/journal.pgen.1000625>.
- Marín-Gual L, González-Rodelas L, Pujol G, Vara C, Martín-Ruiz M, Berríos S, Fernández-Donoso R, Pask A, Renfree MB, Page J, et al. Strategies for meiotic sex chromosome dynamics and telomeric elongation in marsupials. *PLoS Genet*. 2022;**18**(2): e1010040. <https://doi.org/10.1371/journal.pgen.1010040>.
- McDonald J, Kreitman M. Adaptive protein evolution at *Adh* in *Drosophila*. *Nature*. 1991;**351**(6328):652–654. <https://doi.org/10.1038/351652a0>.
- Medarde N, López-Fuster MJ, Muñoz-Muñoz F, Ventura J. Spatio-temporal variation in the structure of a chromosomal polymorphism zone in the house mouse. *Heredity*. 2012;**109**(2): 78–89. <https://doi.org/10.1038/hdy.2012.16>.
- Medarde N, Merico V, López-Fuster MJ, Zuccotti M, Garagna S, Ventura J. Impact of the number of Robertsonian chromosomes on germ cell death in wild male house mice. *Chromosome Res*. 2015;**23**(2):159–169. <https://doi.org/10.1007/s10577-014-9442-8>.
- Mérot C, Stenlökk KSR, Venney C, Laporte M, Moser M, Normandeau E, Áryasi M, Kent M, Rougeux C, Flynn JM, et al. Genome assembly, structural variants, and genetic differentiation between lake whitefish young species pairs (*Coregonus* sp.) with long and short reads. *Mol Ecol*. 2023;**32**(6):1458–1477. <https://doi.org/10.1111/mec.16468>.
- Mihola O, Trachtulec Z, Vlcek C, Schimenti JC, Forejt J. A mouse speciation gene encodes a meiotic histone H3 methyltransferase. *Science*. 2009;**323**(5912):373–375. <https://doi.org/10.1126/science.1163601>.
- Morgan AP, Fu CP, Kao CY, Welsh CE, Didion JP, Yadgary L, Hyacinth L, Ferris MT, Bell TA, Miller DR, et al. The mouse universal genotyping array: from substrains to subspecies. *G3*. 2016;**6**(2): 263–279. <https://doi.org/10.1534/g3.115.022087>.
- Morgan AP, Welsh CE. Informatics resources for the collaborative cross and related mouse populations. *Mamm Genome*. 2015;**26**(9–10): 521–539. <https://doi.org/10.1007/s00335-015-9581-z>.
- Nei M. *Molecular evolutionary genetics*. New York (NY): Columbia University Press; 1987.
- Nei M, Gojobori T. Simple methods for estimating the numbers of synonymous and nonsynonymous nucleotide substitutions. *Mol Biol Evol*. 1986;**3**(5):418–426. <https://doi.org/10.1093/oxfordjournals.molbev.a040410>.
- Noor MAF, Gratos KL, Bertucci LA, Reiland J. Chromosomal inversions and the reproductive isolation of species. *Proc Natl Acad Sci USA*. 2001;**98**(21):12084–12088. <https://doi.org/10.1073/pnas.221274498>.
- Paigen K, Petkov PM. PRDM9 and its role in genetic recombination. *Trends Genet*. 2018;**34**(4):291–300. <https://doi.org/10.1016/j.tig.2017.12.017>.
- Parvanov ED, Petkov PM, Paigen K. *Prdm9* controls activation of mammalian recombination hotspots. *Science*. 2010;**327**(5967): 835. <https://doi.org/10.1126/science.1181495>.
- Piálek J, Hauffe HC, Searle JB. Chromosomal variation in the house mouse. *Biol J Linn Soc*. 2005;**84**(3):535–563. <https://doi.org/10.1111/j.1095-8312.2005.00454.x>.
- Rand DM, Kann LM. Excess amino acid polymorphism in mitochondrial DNA: contrasts among genes from *Drosophila*, mice, and humans. *Mol Biol Evol*. 1996;**13**(6):735–748. <https://doi.org/10.1093/oxfordjournals.molbev.a025634>.
- Reeves A. MicroMeasure: a new computer program for the collection and analysis of cytogenetic data. *Genome*. 2001;**44**(3): 439–443. <https://doi.org/10.1139/gen-44-3-439>.
- Ribagorda M, Berríos S, Solano E, Ayarza E, Martín-Ruiz M, Gil-Fernández A, Parra MT, Viera A, Rufas JS, Capanna E, et al. Meiotic behavior of a complex hexavalent in heterozygous mice for Robertsonian translocations: insights for synapsis dynamics. *Chromosoma*. 2019;**128**(2): 149–163. <https://doi.org/10.1007/s00412-019-00695-8>.
- Rieseberg LH. Chromosomal rearrangements and speciation. *Trends in Ecology and Evolution*. 2001;**16**(7):351–358. [https://doi.org/10.1016/S0169-5347\(01\)02187-5](https://doi.org/10.1016/S0169-5347(01)02187-5).
- Robertson WRB. Chromosome studies. I. Taxonomic relationships shown in the chromosomes of tettigidae and acrididae: V-shaped chromosomes and their significance in acrididae, locustidae, and gryllidae: Chromosomes and variation. *J Morphol*. 1916;**27**(2):179–331. <https://doi.org/10.1002/jmor.1050270202>.
- Romanienko PJ, Camerini-Otero RD. The mouse Spo11 gene is required for meiotic chromosome synapsis. *Mol Cell*. 2000;**6**(5): 975–987. [https://doi.org/10.1016/S1097-2765\(00\)00097-6](https://doi.org/10.1016/S1097-2765(00)00097-6).
- Rozas J, Ferrer-Mata A, Sanchez-DelBarrio JC, Guirao-Rico S, Librado P, Ramos-Onsins SE, Sanchez-Gracia A. DnaSP 6: DNA sequence polymorphism analysis of large data sets. *Mol Biol Evol*. 2017;**34**(12):3299–3302. <https://doi.org/10.1093/molbev/msx248>.
- Ruiz-Herrera A, Vozdova M, Fernández J, Sebestova H, Capilla L, Frohlich J, Vara C, Hernández-Marsal A, Sipek J, Robinson TJ, et al. Recombination correlates with synaptonemal complex length and chromatin loop size in bovids—insights into mammalian meiotic chromosomal organization. *Chromosoma*. 2017;**126**(5):615–631. <https://doi.org/10.1007/s00412-016-0624-3>.
- Sandor C, Li W, Coppieters W, Druet T, Charlier C, Georges M. Genetic variants in REC8, RNF212, and PRDM9 influence male recombination in cattle. *PLoS Genet*. 2012;**8**(7):e1002854. <https://doi.org/10.1371/journal.pgen.1002854>.
- Sans-Fuentes MA, García-Valero J, Ventura J, López-Fuster MJ. Spermatogenesis in house mouse in a Robertsonian polymorphism zone. *Reproduction*. 2010;**140**(4):569–581. <https://doi.org/10.1530/REP-10-0237>.
- Sayers EW,avanaugh M, Clark K, Pruitt KD, Sherry ST, Yankie L, Karsch-Mizrachi I. GenBank 2024 update. *Nucleic Acids Res*. 2023;**2023**:134–137. <https://doi.org/10.1093/nar/gkad903>.
- Schwarz T, Striedner Y, Horner A, Haase K, Kempfner J, Zeppezauer N, Hermann P, Tiemann-Boege I. PRDM9 forms a trimer by interactions within the zinc finger array. *Life Science Alliance*. 2019;**2**(4):1–14. <https://doi.org/10.26508/lsa.201800291>.
- Segura J, Ferretti L, Ramos-Onsins S, Capilla L, Farré M, Reis F, Oliver-Bonet M, Fernández-Bellón H, García F, García-Caldés M, et al. Evolution of recombination in eutherian mammals: insights into mechanisms that affect recombination rates and crossover interference. *Proc R Soc B Biol Sci*. 2013;**280**:1771. <https://doi.org/10.1098/rspb.2013.1945>.
- Smagulova F, Gregoret IV, Brick K, Khil P, Camerini-Otero RD, Petukhova GV. Genome-wide analysis reveals novel molecular features of mouse recombination hotspots. *Nature*. 2011;**472**(7343):375–378. <https://doi.org/10.1038/nature09869>.
- Tajima F. Statistical method for testing the neutral mutation hypothesis by DNA polymorphism. *Genetics*. 1989;**123**(3): 585–595. <https://doi.org/10.1093/genetics/123.3.585>.
- Thomas PD, Campbell MJ, Kejariwal A, Mi H, Karlak B, Daverman R, Diemer K, Muruganujan A, Narechania A. PANTHER: a library of protein families and subfamilies indexed by function. *Genome Res*. 2003;**13**(9):2129–2141. <https://doi.org/10.1101/gr.772403>.
- Tock AJ, Henderson IR. Hotspots for initiation of meiotic recombination. *Front Genet*. 2018;**9**:511. <https://doi.org/10.3389/fgene.2018.00521>.

- Vara C, Capilla L, Ferretti L, Ledda A, Sánchez-Guillén RA, Gabriel SI, Albert-Lizandra G, Florit-Sabater B, Bello-Rodríguez J, Ventura J, et al. PRDM9 diversity at fine geographical scale reveals contrasting evolutionary patterns and functional constraints in natural populations of house mice. *Mol Biol Evol.* 2019;**36**(8): 1686–1700. <https://doi.org/10.1093/molbev/msz091>.
- Vara C, Paytuví-Gallart A, Cuartero Y, Álvarez-González L, Marín-Gual L, García F, Florit-Sabater B, Capilla L, Sánchez-Guillén RA, Sarrate Z, et al. The impact of chromosomal fusions on 3D genome folding and recombination in the germ line. *Nat Commun.* 2021;**12**(1):1–17. <https://doi.org/10.1038/s41467-021-23270-1>.
- Vara C, Ruiz-Herrera A. Unpacking chromatin remodelling in germ cells: implications for development and evolution. *Trends Genet.* 2022;**38**(5):422–425. <https://doi.org/10.1016/j.tig.2021.10.007>.
- Vasco C, Manterola M, Page J, Zuccotti M, De La Fuente R, Redi CA, Fernandez-Donoso R, Garagna S. The frequency of heterologous synapsis increases with aging in Robertsonian heterozygous male mice. *Chromosome Res.* 2012;**20**(2):269–278. <https://doi.org/10.1007/s10577-011-9272-x>.
- Wallace BMN, Searle JB, Everett CA. Male meiosis and gametogenesis in wild house mice (*Mus musculus domesticus*) from a chromosomal hybrid zone; a comparison between “simple” robertsonian heterozygotes and homozygotes. *Cytogenet Genome Res.* 1992;**61**(3):211–220. <https://doi.org/10.1159/000133410>.
- Wallace BMN, Searle JB, Everett CA. The effect of multiple simple Robertsonian heterozygosity on chromosome pairing and fertility of wild-stock house mice (*Mus musculus domesticus*). *Cytogenet Genome Res.* 2002;**96**(1–4):276–286. <https://doi.org/10.1159/000063054>.
- Wang S, Liu Y, Shang Y, Zhai B, Yang X, Kleckner N, Zhang L. Crossover interference, crossover maturation, and human aneuploidy. *BioEssays.* 2019;**41**(10):1800221. <https://doi.org/10.1002/bies.201800221>.
- Wellenreuther M, Bernatchez L. Eco-evolutionary genomics of chromosomal inversions. *Trends Ecol Evol.* 2018;**33**(6):427–440. <https://doi.org/10.1016/j.tree.2018.04.002>.
- White MJD. *Animal cytology and evolution*. Cambridge: Cambridge University Press; 1973.
- White MA, Wang S, Zhang L, Kleckner N. Quantitative modeling and automated analysis of meiotic recombination. *Methods Mol Biol.* 2017;**1471**:305–323. https://doi.org/10.1007/978-1-4939-6340-9_18.
- Yoshida K, Rödelberger C, Röseler W, Riebesell M, Sun S, Kikuchi T, Sommer RJ. Chromosome fusions repatterned recombination rate and facilitated reproductive isolation during *Pristionchus* nematode speciation. *Nat Ecol Evol.* 2023;**7**(3):424–439. <https://doi.org/10.1038/s41559-022-01980-z>.